ADVANCED FUNCTIONAL MATERIALS
www.afm-journal.de

Materials Views
www.MaterialsViews.com

Structure–Property Relations in All-Organic Dye-Sensitized Solar Cells

*Yang Jiao, Fan Zhang, Michael Grätzel, and Sheng Meng**

A structure–property relationship in all-organic dye solar cells is revealed by first-principles molecular dynamics and real-time time-dependent density functional theory simulations, accompanied with experimental confirmation. An important structural feature at the interface, Ti–N anchoring, for a broad group of all-organic dyes on TiO_2 is inferred from energetics, vibrational recognition, and electronic data. This fact is contrary to the usual assumption; however, it optimizes electronic level alignment and photoelectron injection dynamics, greatly contributing to the observed efficiency improvement in all-organic cyanoacrylate dye sensitized solar cells.

1. Introduction

As one of the most promising alternative to more costly single-crystal photovoltaic devices, dye-sensitized solar cells (DSSCs) have received increasing attention in recent years.[1–3] High sunlight-to-current conversion efficiency, over 12%,[3,4] and long-term stability[5] have been achieved. Applications of DSSCs in building integrated photovoltaics have been started.[2] Dye sensitizers play a critical role for further improving photovoltaic performance towards large-scale implementation in the near future. Metal complexes, such as Ru-complex N719, are prototype sensitizers producing a high efficiency of 11.9%.[3] However, cost and environmental concerns have led to the rapid development of all-organic metal-free dyes having high extinction coefficient, nontoxicity, and easy fabrication.[6–8] DSSCs employing all-organic dyes have reached energy conversion efficiencies of 10.3%,[6] and recently 12.3% with a newly developed porphyrin dye;[4] these are comparable to the efficiencies achieved using toxic metal complexes and thus are promising for practical large-scale implementation.

The most popular all-organic dyes utilize a donor–π–acceptor (D-π-A) structure, for efficient electron injection and hindered recombination. A cyanoacrylic group is the most commonly used acceptor. Examples include triphynilamine dye L2 (also referred to as D5) synthesized in 2006, which employs the triphynilamine group as the donor and cyanoacrylic group as the acceptor.[9] Various modifications on the donor and the π linker of the dye have been tested,[10] among which the C219 dye with a dithienosilole linker was reported to yield the efficiency of 10.3%.[6] A recent breakthrough reports a record efficiency of 12.3% using porphyrin-based D-π-A structures and cobalt-based electrolytes.[4]

However, despite a tremendous number of experimental studies on macroscopic properties such as film morphology, spectroscopy, and current–voltage curves, a microscopic picture of the anchoring state of these all-organic metal-free dyes on TiO_2 photoanodes is still lacking. Controversy exists concerning the dyes' adsorption sites.[7,11] This is different from the situation for metal-complex dyes, where experimental[12,13] and theoretical analyses[14–16] revealed that N719 and derivatives bind onto anatase (101) via one to three carboxylic/carboxylate groups forming bidentate or monodentate for each group. Intuitively, it is widely assumed that all-organic cyanoacrylic dyes also bind the TiO_2 surface through their carboxylic group, similar to N719.[17] Photoelectron spectroscopy experiments confirmed that adsorbed L2 dye has its cyanoacrylic acceptor staying close to the surface and its donor pointing away from the surface.[11] The cyano group, on the other hand, was considered to act purely as an electron-drawing acceptor, which does not directly bind TiO_2 and has no contribution to interface stability.[7,11] Without solid characterization of the binding geometry of all-organic cyanoacrylic dyes on a prototypical anatase (101) surface, a complete understanding of the working mechanism of DSSCs and details about interface charge separation and recombination cannot be achieved; further optimization of all-organic dye devices will be hindered by these missing details.[18,19]

Here we have systematically studied the adsorption structure of all-organic cyanoacrylic dyes on TiO_2 in vacuum and in solution. Based on extensive searches for the ground-state geometry and molecular dynamics (MD) simulations, we found that the tridentate adsorption forming interface Ti–N bonds is energetically and dynamically stable, and that the corresponding vibrational spectrum is in good agreement with infrared spectroscopy experiments.[7,8] We also study the effects of Ti–N bonding on photovoltaic performance to explore associated structure-property relationships in all-organic DSSCs. The bonding largely accounts for the stabilized dye anchoring, enhanced

Y. Jiao, F. Zhang, Prof. S. Meng
Beijing National Laboratory for Condensed Matter Physics
Institute of Physics
Chinese Academy of Sciences
Beijing 100190, P. R. China
E-mail: smeng@iphy.ac.cn
Prof. M. Grätzel
Laboratory of Photonics and Interfaces
Swiss Federal Institute of Technology (EPFL)
CH-1015 Lausanne, Switzerland

DOI: 10.1002/adfm.201201831

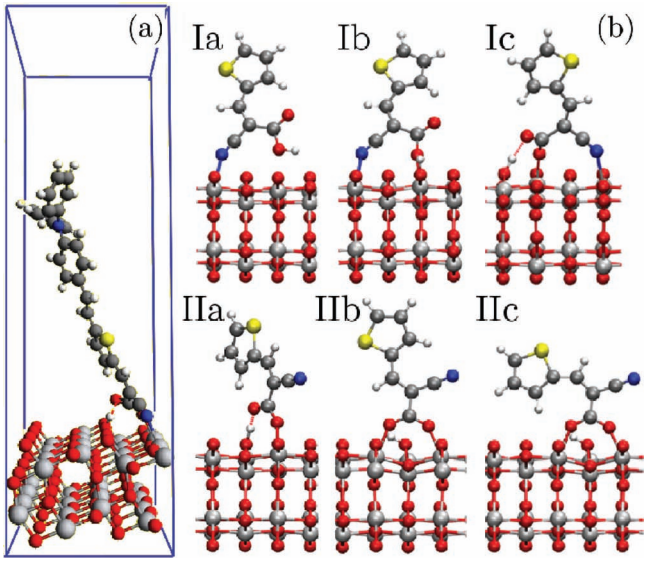

Figure 1. a) The unit cell with L2 dye on TiO_2 anatase (101) used in the calculations. b) Different adsorption structures of the M0 model molecule. First row: adsorption with Ti–N bonding; second row: adsorption without Ti–N bonds.

open-circuit voltage (V_{oc}), and ultrafast photoelectron injection with high yield observed in experiments.[6,17] Such a fundamental understanding of interface atomistic structure is vital to unravel the microscopic mechanisms for energy conversion in the new generation of energy devices, as well as providing the basis for practical implementations, such as adjusting surface acidity to favor selectively interface Ti–N bonding.

2. Results and Discussion

Figure 1a shows a representative model for dye adsorption with the unit cell depicted as straight lines. A six-layer (2×4) TiO_2 slab is used to model the anatase (101) surface, where the bottom three layers are fixed in their bulk geometry. We adopt calculated lattice constant of $a = b = 3.82$ Å, and $c = 9.66$ Å, which agree well with experimental values of 3.79 and 9.51 Å.[20] The slab is separated by a vacuum layer of more than 20 Å from its images, and dipole correction is employed to cancel artificial interactions between them. This model gives a reliable description of surface electronic structure, judged by resemblance to that for thicker slabs (15-layer). For the dye, we choose L2 as our model, since it has a simple structure while keeping a relative high efficiency of around 6%.[9] Dye concentration in this model is 1.05 μmol m^{-2}, comparable to typical surface coverages in experiment.[23]

2.1. Atomistic Interface Structure

We first investigate all possible adsorption configurations of D-π-A cyanoacrylic dyes on anatase (101). Since the interaction between dyes and TiO_2 is localized at the acceptor part of the dye, we adopt a smaller model M0, which is cut from L2 at the thiophene moiety (Figure 1b). This segment contains the same acceptor as all other important cyanoacrylic dyes; and the heavy computational cost is alleviated thanks to its small size. We checked that this model gives a reliable description of binding geometry and electronic structure near conduction band minimum (CBM). The lowest unoccupied molecular orbital (LUMO) is localized on the cyanoacrylic acceptor, and its distribution is the same as for L2 adsorption.

Among many possible adsorption configurations, a few representative ones are shown in Figure 1b. They can be arranged into two groups: i) those with the cyano group –CN bonded to the substrate (upper row) and ii) those with free –CN (lower row). Configuration Ia is intact adsorption with only –CN bonded to the surface, while all others have the H of carboxylic group transferred to surface O. Ib has both –CN and –CO bonded to surface. Ic is more robust with an additional hydrogen bond (H-bond) connected to the surface. IIa is bonded by the Ti–O monodentate and an H-bond. Structures IIb and IIc have the same bidentate adsorption conformer with two interface Ti–O bonds but at a different molecular orientation: IIc has the thiophene group twisted and closer to TiO_2 surface. The bidentate IIb and IIc configurations are most studied in the literature and were always thought to be the most stable.[7] To our surprise, accurate ab initio calculations show that the most stable geometry is Ic instead of IIb/IIc. The adsorption energy for Ic is 0.2–0.4 eV larger than those with carboxylate bidentate anchors (see **Table 1**). This can be understood since Ic involves a stable tridentate bonding. Adsorption energies are consistent with calculated bond strength for Ti–N, Ti–O and H-bonds (aproximately 0.7, 0.6, and 0.3 eV, respectively). This confirms the crucial role of Ti–N bonds in maintaining the interface stability of cyanoacrylic dye solar cells.

To explore their dynamic stability, MD simulations of these configurations at 300 K were performed. **Figure 2** shows the time evolution of anchor bond lengths. Bonds in configurations Ic and IIb/IIc are found stable, oscillating around their equilibrium values during the entire 6 ps trajectory. The average Ti–O bond length in Ic is 2.02 Å, while for bidentate adsorption in IIc Ti–O bonds vibrate around 2.10 Å with an amplitude of approximately 0.2 Å, indicating a stronger bond in the former. The Ti–N and H-bond have greater oscillations but still maintain their stability. On the other hand, some configurations tend to transform into tridentate Ic mode. In Ib the free –CO binds to surface H, forming an H-bond and changes to Ic within 1 ps. In IIa the cyano group, initially far away from the surface (shown by the Ti–N distance of over 6 Å), binds the five-folded surface Ti at approximately 3.2 ps forming a Ti–N

Table 1. Adsorption energy (E_{ads}) and geometry parameters for all configurations on TiO_2.

	Ia	Ib	Ic	IIa	IIb	IIc
E_{ads} [eV]	0.731	1.121	1.426	0.932	1.233	1.010
d_{Ti-N} [Å]	2.296	2.240	2.268	–	–	–
d_{Ti-O} [Å]	2.744	1.943	2.026	2.017	2.082	2.084

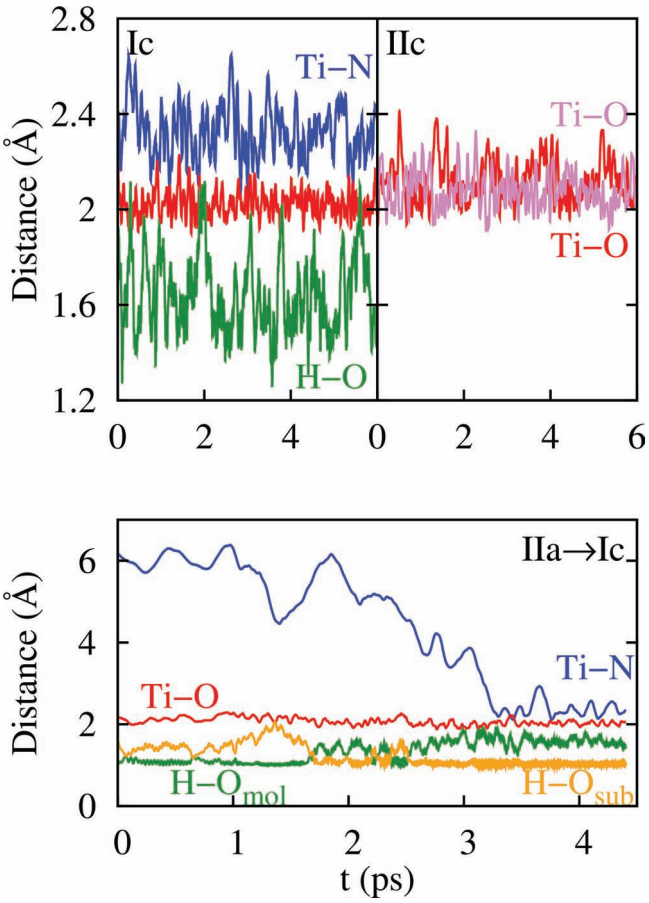

Figure 2. Evolution of anchoring bond lengths in adsorption configurations Ic, IIc, and IIa. IIa changes into Ic at about 3.2 ps in MD simulations.

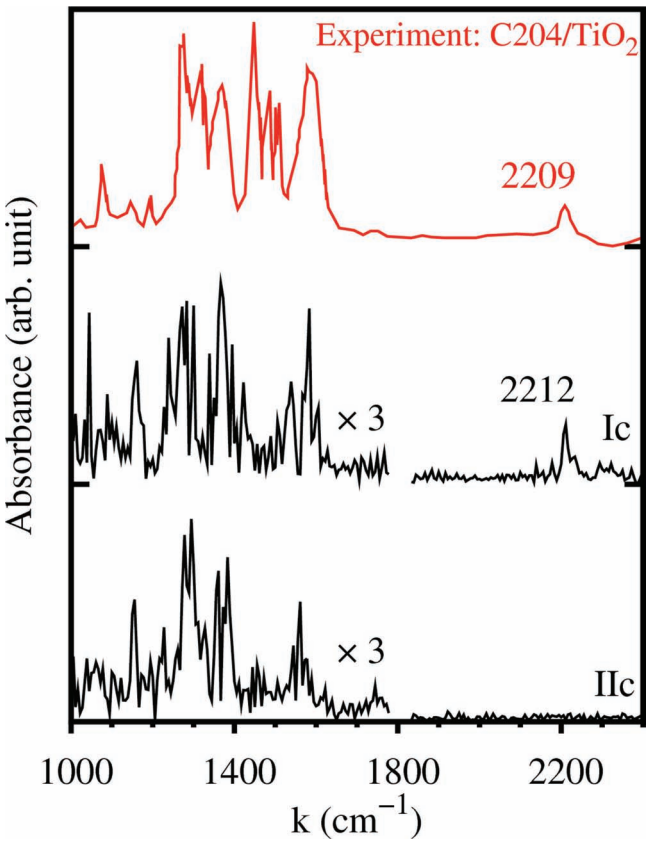

Figure 3. Experimental and theoretical vibrational spectra for cyanoacrylic dye adsorption. The red line is from experimental infrared spectroscopy using C204 dye.[7] The black lines are from the Fourier transforms of dipole moment evolution for configurations Ic and IIc in MD simulations. The calculated spectrum at low energies is multiplied by a factor of 3 to mimic roughly 3 times increase in molecular size from M0 to C204.

bond at a distance of 2.4 Å. During this process, the carboxylic group transfers its proton to the surface O and gets deprotonated, while maintaining the interface Ti–O bond; the configuration thus transforms into Ic (Figure 2, IIa → Ic). If configurations IIb and IIc first change into IIa, transformation of IIb/IIc → Ic via IIa might also occur, with an approximate barrier of 0.3 eV. Other configurations such as Ia can easily convert to Ic by rotating around the Ti–N bond and carboxyl group binding. To conclude, Ic might be the only thermodynamically stable state concerning cyanoacrylic group anchoring. Our MD simulations including acetonitrile molecules show that the anchor bonds in Ic are not disrupted by solvents (see Figure S1 in the Supporting Information).

2.2. Confirmation by Experiment: Vibrational Recognition

Direct comparison to experiment can be performed by vibrational spectroscopy analysis. Vibration spectra, obtained by Fourier transform of the dipole correlation function in MD trajectories, are shown in **Figure 3**. For comparison, the experimental infrared absorption spectrum for a similar dye C204 with the same anchor on TiO_2 is also presented.[7] We focus on modes within 1000–2500 cm^{-1}, which mainly come from the molecular skeleton, including the anchor group. Features around 1450 cm^{-1} come from the donor part of C204, and are absent for the simplified model M0. We found that the spectrum for Ic is very close to experiment, while there are some discrepancies between spectrum for IIc and the experiment. For example, there are around 3 small peaks below 1200 cm^{-1}, and a big bump in the range of 1250–1600 cm^{-1} for both experiment and the spectrum for Ic configuration.

More prominent is the feature at around 2200 cm^{-1}, shown in both experiment and the Ic spectrum but is absent for IIc. This mode corresponds to –CN stretching; since in IIc the cyano group is unbound and sticking out almost parallel to the surface, its contribution to the dipole moment along surface normal is minimal, leading to a small amplitude buried in the noisy background in vibration spectrum. Taking this peak as a reference, the calculated intensity for vibrations at 1000–1600 cm^{-1} is relatively low compared to the experimental spectrum, because the modified model dye M0 is significantly smaller than the C204 dye used in experiment (roughly 3 times smaller). Previously the presence of –CN mode at around 2200 cm^{-1}, with the same frequency as that for free dyes in solution, was believed to indicate that –CN does not bind to the TiO_2 surface.[7,6] By monitoring the –CN bond length in MD

simulations, we found the surface-bonded –CN in Ic yields a frequency of 2212 cm^{-1}, very close to that for a free, unbound –CN in IIc, 2217 cm^{-1}. Despite there being no significant shift in –CN stretching thanks to the very strong –C≡N triple bond, consistent with previous observations,[7]–CN does show a small but finite frequency shift after surface binding.

Motivated by theoretical predictions, we conducted experimental investigations to measure the vibration properties of –CN groups in the presence of TiO_2 nanoparticles. To this regard, we measure the infrared spectrum of model dye molecules with a cyanoacrylic group (2-cyano-3-thiophene acrylic acid) and that with only cyano-group as a potential anchor (4-chloro cinnamonitrile), in free solution and on TiO_2. The latter molecule is intended to eliminate the influence of –COO(H) group during dye adsorption. In both cases we found strong evidence that the –CN stretch mode shifts to new frequencies due to surface Ti–N bonding (see Figure S2 in the Supporting Information). For the molecule with the cyanoacrylic anchor, –CN stretching shifts from 2225 in free powder to 2222 cm^{-1} on TiO_2, in agreement with the 5 cm^{-1} shift predicted above from first-principles for M0. In addition, a shoulder at 1150 cm^{-1} shows up upon surface adsorption, which is absent for both free dyes and bare TiO_2. Through theoretical analysis this mode is attributed to C–C stretching of the cyanoacrylic group after surface binding. More importantly, molecules with only a –CN group and no carboxyl anchor also show a dramatic shift in –CN stretching, suggesting unambiguously the presence of surface Ti–N bonds. For 4-chloro cinnamonitrile, the –CN stretch shifts from 2218 cm^{-1} in free powder to 2225 cm^{-1} on TiO_2, consistent with our calculation. This shift is a result of Ti–N bonding without carboxyl anchoring. Direct observation of Ti–N vibrations, located at 650 cm^{-1}, is blocked, unfortunately, due to the appearance of strong TiO_2 vibration modes centered at 600–800 cm^{-1} (see Figure S2).

More evidence come from the vibration modes of the carboxylate group. The frequency difference ($\Delta\nu$) between the asymmetric (ν_{asym}) and symmetric (ν_{sym}) vibration mode of $–COO^-$ moiety can serve as a fingerprint to discern anchoring geometries.[21] Subtraction and summation of the two C–O bond lengths are used to represent the asymmetric and symmetric vibrational modes, respectively. For Ic, they are located at 1580 and 1275 cm^{-1}, respectively, leaving $\Delta\nu$ = 300 cm^{-1}. For IIc, the two modes are at 1562 and 1296 cm^{-1}, with $\Delta\nu$ = 264 cm^{-1}. These values are summarized in **Table 2**, together with similar assignments on available experimental data. The experiments are performed for dyes all having the cyanoacrylic acceptor. Clearly, the Ic configuration presents a $\Delta\nu$ close to those measured (304–313 cm^{-1}), indicating this configuration is dominant.

Table 2. Frequencies for asymmetric and symmetric – COO^- vibration and their difference $\Delta\nu$ between experimental and theoretical spectra.

Dye		ν_{asym} [cm^{-1}]	ν_{sym} [cm^{-1}]	$\Delta\nu$ [cm^{-1}]	Ref.
C204		1578	1272	306	[7]
C205		1572	1266	306	[7]
TPC1		1587	1283	304	[21]
NKX2311		1581	1268	313	[8]
M0	in Ic	1583	1283	300	This work
M0	in IIc	1562	1298	264	This work

2.3. Band Offsets and Open Voltage

The dominant presence of Ic configuration, with the appearance of previously ignored Ti–N bonds, also proves critical for the performance of photovoltaic devices, in terms of interface band alignment and photoelectron injection efficiency, as discussed below. We found that interface Ti–N bonds result in an optimal band alignment at the interface, namely, an upshifted and closer TiO_2 CBM relative to dye LUMO, leading to enhanced V_{oc}[17] and minimized kinetic redundancy[22] in photovoltaic devices comparing to those configurations without interface Ti–N bonds. This is consistent with the general observations that the measured V_{oc} could be as high as 1.1 V using cyanoacrylic dyes in solid-state electrolyte.[17]

The interface geometry has a significant impact on the electronic structure of the dye/TiO_2 system. It is well known that the latter could be modified by adsorption of polar molecules.[23–25] For example, the CBM of semiconductor will be upshifted by introducing a positive surface dipole. For convenience, to characterize the band alignment at the interface we define band level difference as $\Delta E = E_{LUMO} - E_{CBM}$, which is the difference between the energy level of the dye's LUMO and the CBM of the semiconductor. We emphasize that a small but positive ΔE is optimal for DSSC, leading to minimized kinetic redundance.[22] For instance, detailed analysis shows that TiO_2 CBM is upshifted toward vacuum level when decreasing ΔE, resulting in enhanced V_{oc}.

Figure 4 shows that ΔE is a linear function of surface dipole moment induced by dye adsorption. For all cases except Ia, ΔE shifts by –0.228 eV e^{-1} $Å^{-1}$. with respect to surface dipole moment. A similar effect was observed experimentally for coadsorption albeit with a smaller slope.[24] However, the Ia case is distinct, which does not follow this trend. We then construct two new interface configurations similar to Ia but with

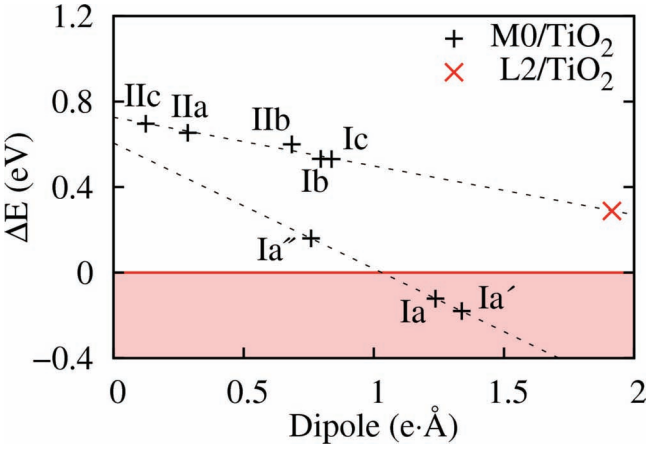

Figure 4. Band level difference ΔE as a function of surface dipole moment in different configurations. $\Delta E = E_{LUMO} - E_{CBM}$.

a different orientation (IIa' and IIa"); for these three cases ΔE shifts linearly with surface dipole moment with a different slope of –0.588 eV e^{-1} $Å^{-1}$. We attribute this difference between the latter three configurations and all other cases to the difference in surface states upon adsorption, namely the absence of surface protonation in the Ia cases. The same trend would occur for complete dye L2: the calculated ΔE for L2 in Ic configuration is 0.288 eV and follows the same line as M0 (the red cross in Figure 4). Therefore we find that different adsorption modes adjust ΔE in a different way, due to differences in electronic coupling strength.

2.4. Ultrafast Electron Injection and Photocurrent

We also analyze the influence of interface Ti–N bonds on the efficiency of photoelectron injection by performing TDDFT electron–ion dynamics simulation. Configurations both with (Ic) and without interface Ti–N bonds (IIb and IIc) are considered. **Figure 5** displays χ, the ratio of excited state distributed onto TiO_2 substrate, as a function of time after photoexcitation. There exhibits an ultrafast electron injection process for all three cases considered here. For Ic, the excited electron starts to inject into the TiO_2 conduction band at approximately 16 fs, and finishes at about 100 fs. The curve can be fitted by an exponential $\chi = 0.705–0.665\exp(-t/64)$ for $t \geq 16$ fs. From Figure 5 we infer that the photoexcited state undergoes an ultrafast electron transfer from dyes to the TiO_2 electrode within a timescale of 64 fs. The density of excited electron distributes over both Ti–N and Ti–O bonds during injection, implying both serve as conducting channels for photoelectron injection.

Following the same analysis we find similar and slightly faster timescale for photoelectron injection for IIb and IIc configurations: the obtained injection time is 59 fs fitting the simulation data. Note that IIc configuration exhibits a linear-like dependence

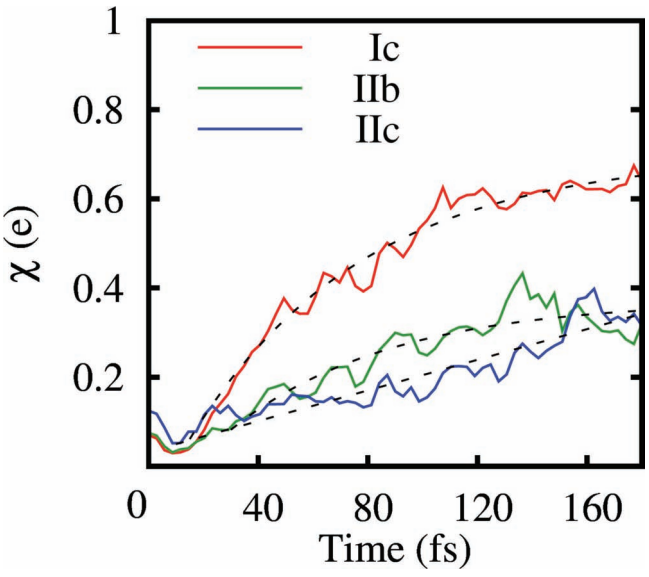

Figure 5. Electron injection dynamics for configurations Ic, IIb, and IIc from coupled electron–ion MD simulation based on TDDFT. Dotted lines are fitted by an exponential function.

of injected electron on time, which we attribute to the influence of the dye's twisted thiophene group that is close to the substrate and may interact with the injected electron. Nevertheless, the overall injection timescale is very close to IIb. The injection times of 59 and 64 fs are compatible with observed experimental values ranging from 30 fs to a few hundred fs for ultrafast photoelectron injection using cyanoacrylic dyes.[27] Comparing to the lifetime of excited states in all-organic dyes ($\tau_{lifetime} \approx$ 1–100 ps), the ultrashort injection time suggests an electron injection efficiency $\eta_{inj} = 1 - \tau_{inj}/\tau_{lifetime} \geq 94\%$. Note that although IIb and IIc configurations produce larger driving forces (ΔE) for photoelectron injection (at the cost of lower V_{oc}), the gain in injection efficiency η_{inj} is minimal since η_{inj} is already very close to 100%. Another significant advantage of Ic configuration is that it has a larger quantum yield (equilibrium photoelectron fraction) after injection, 70% comparing to 37% for IIb and IIc. This reflects the electronic coupling at the interface in IIb and IIc configurations being too strong, such that substantial state mixing between the dye LUMO and TiO_2 conduction band occurs. The quantum yield for electron injection is almost doubled in the Ic case, as a result of adjusting dye's LUMO level towards the semiconductor CBM by the formation of interface Ti–N bond.

Therefore the presence of interface Ti–N bonds is beneficial for all-organic cyanoacrylic dyes, producing stable dye anchoring and higher V_{oc} while maintaining efficient photoelectron injection with higher yields. Improvement in efficiency might be expected if more ordered dye/TiO_2 interface with dominant Ic configurations are prepared or by adding –CN to cyano-free anchors. Extensive interface engineering and procedure optimization during fabrication of solar cell materials and devices, for instance, by prolonged substrate heating, introducing surface defects, or adjusting the pH of the TiO_2 interface,[22] may be used to promote surface Ti–N bonding while blocking formation of other competing configurations. However, our major finding here is that the cyano group in all-organic cyanoacrylic dyes is not just an electron-accepting unit, but also an extra anchoring group that contributes to interface stability and electron injection.

3. Conclusions

Extensive theoretical analysis and comparison to experiment reveal consolidated evidence for tridentate adsorption of all-organic cyanoacrylic dyes featuring Ti–N bonding in DSSC. This unappreciated interface geometry is responsible for producing optimal band alignment to minimize kinetic redundance, retaining ultrafast photoelectron injection with high yield, and stable anchoring at room temperature, thus rendering outstanding photovoltaic properties such as high V_{oc}, high efficiency, and stability which are observed in experiment for DSSCs based on all-organic D-π-A dyes.[6,17] The results also point to effective strategies for dye design and device optimization, for example, by managing the adsorption geometry to favor interface Ti–N bonds.

4. Experimental Section

Theoretical Computation: The calculations are based on first-principles MD and electron dynamics simulation within the framework of density functional theory (DFT) and time-dependent DFT (TDDFT). MD studies

were performed with VASP, using Vanderbilt ultrasoft pseudopotentials and generalized gradient approximation of PW91 and HSE for exchange-correlation energy.[28,29] An energy cutoff of 400 eV and Γ point *k*-sampling is used, together with a Gaussian smearing width of 0.1 eV. This set of parameters gives an energy convergence of less than 0.01 eV atom^{-1}. In MD simulations, a time step of 1 fs is used. The system is equilibrated for 1 ps followed by a 6 ps production run, yielding vibration spectroscopy with an energy resolution of 6 cm^{-1} by Fourier transform of the dipole correlation function. Photoelectron dynamics is monitored by a coupled electron–ion evolution method,[30,31] where electronic wavefunctions are propagated by real-time TDDFT after promoting an electron from the dye's highest occupied molecular orbital (HOMO) to the LUMO, modeling the first excited state. The coupled electron–ion system is propagated by 6000 steps with a time step of 0.024 fs. Note that to model such a realistic interface from first principles the molecular and electronic dynamics simulation is computationally demanding: a single 6000-step trajectory takes about 160 cpu-days on Intel Xeon processors.

Sample Preparation: The Degussa P25 TiO_2 nanoparticles (3.5 g, 99.5%) is dispersed in ethanol (AR grade, 25 mL) to form a uniform suspension. The TiO_2 paste is then spread out onto pre-cleaned glasses by the doctor-blade method and sintered at 450 °C for 30 min. In the meantime, 2-cyano-3-thiophene acrylic acid (PI Company, 97%) is dissolved in ethanol to obtain a solution (5 mM). For 4-chloro cinnamonitrile (Sigma Aldrich, 98%), a solution with ethanol solvent (20 mM) is prepared. When the TiO_2 paste cools down to 100 °C, the films are immersed into the prepared solutions in darkness for at least 6 h to load dye molecules onto TiO_2 surface. Before Fourier transform infrared (FTIR) spectroscopy measurement, cyanoacrylic acid-adsorbed TiO_2 is rinsed by ethanol to remove unbound molecules and left to dry in air. TiO_2 film immersed in 4-chloro cinnamonitrile ethanol solution is allowed to dry directly in air.

FTIR Spectroscopy Measurement: Infrared spectra are obtained using a Nicolet iN10 MX FTIR spectrometer, produced by Thermo Scientific, USA. A small amount of TiO_2 powder adsorbed with 2-cyano-3-thiophene acrylic acid or 4-chloro cinnamonitrile is scratched away from the glass substrate and pressed between two diamond windows. Spectra covering the range of 4000 cm^{-1} to 600 cm^{-1} with 16 scans are collected. The area under infrared illumination is 100 μm × 100 μm.

Supporting Information

Supporting Information is available from the Wiley Online Library or from the author.

Acknowledgements

The authors acknowledge Dr. F. Shi for assistance in experiment, and financial support from the NSFC (grant 11074287), the MOST (2012CB921403), and the hundred-talent program of CAS.

Received: July 4, 2012
Published online: August 28, 2012

[1] B. O'Regan, M. Grätzel, *Nature* **1991**, *353*, 737.
[2] M. K. Nazeeruddin, E. Baranoff, M. Grätzel, *Sol. Energy* **2011**, *85*, 1172.
[3] M. Grätzel, *Acc. Chem. Res.* **2009**, *42*, 1788.
[4] a) A. Yella, H.-W. Lee, H. N. Tsao, C. Yi, A. K. Chandiran, Md. K. Nazeeruddin, E. W.-G. Diau, C.-Y. Yeh, S. M. Zakeeruddin, M. Grätzel, *Science* **2011**, *334*, 629; b) M. D. McGehee, *Science* **2011**, *334*, 607.
[5] P. Wang, S. M. Zakeeruddin, J. E. Moser, M. K. Nazeeruddin, T. Sekiguchi, M. Grätzel, *Nat. Mater.* **2003**, *2*, 402.
[6] W. Zeng, Y. Cao, Y. Bai, Y. Wang, Y. Shi, M. Zhang, F. Wang, C. Pan, P. Wang, *Chem. Mater.* **2010**, *22*, 1915.
[7] M. Xu, S. Wenger, H. Bala, D. Shi, R. Li, Y. Zhou, S. M. Zakeeruddin, M. Grätzel, P. Wang, *J. Phys. Chem. C* **2009**, *113*, 2966.
[8] K. Hara, T. Sato, R. Katoh, A. Furube, Y. Ohga, A. Shinpo, S. Suga, K. Sayama, H. Sugihara, H. Arakawa, *J. Phys. Chem. B* **2003**, *107*, 597.
[9] D. P. Hagberg, T. Edvinsson, T. Marinado, G. Boschloo, A. Hagfeldt, L. Sun, *Chem. Commun.* **2006**, 2245.
[10] J. K. Lee, S. M. Lee, S. B. Lee, K. H. Kim, S. E. Cho, S. Jang, S. H. Park, W. P. Hwang, M. H. Seo, M. R. Kim, *Curr. Appl. Phys.* **2011**, *11*, S140.
[11] E. M. J. Johansson, T. Edvinsson, M. Odelius, D. P. Hagberg, L. Sun, A. Hagfeldt, H. Siegbahn, H. Rensmo, *J. Phys. Chem. C* **2007**, *111*, 8580.
[12] H. Němec, J. Rochford, O. Taratula, E. Galoppini, P. Kužel, T. Polívka, A. Yartsev, V. Sundström, *Phys. Rev. Lett.* **2010**, *104*, 197401.
[13] C. E. Patrick, F. Giustino, *Phys. Rev. B* **2011**, *84*, 085330.
[14] S. Fantacci, F. De Angelis, A. Selloni, *J. Am. Chem. Soc.* **2003**, *125*, 4381.
[15] F. De Angelis, S. Fantacci, A. Selloni, M. K. Nazeeruddin, M. Grätzel, *J. Phys. Chem. C* **2010**, *114*, 6054.
[16] M. K. Nazeeruddin, F. De Angelis, S. Fantacci, A. Selloni, G. Viscardi, P. Liska, S. Ito, B. Takeru, M. Grätzel, *J. Am. Chem. Soc.* **2005**, *127*, 16835.
[17] P. Chen, J. H. Yum, F. De Angelis, E. Mosconi, S. Fantacci, S. J. Moon, R. H. Baker, J. Ko, Md. K. Nazeeruddin, M. Grätzel, *Nano Lett.* **2009**, *9*, 2487.
[18] L. M. Liu, S. C. Li, H. Cheng, U. Diebold, A. Selloni, *J. Am. Chem. Soc.* **2011**, *133*, 7816.
[19] T. L. Bahers, F. Labat, T. Pauporte, P. P. Laine, I. Ciofini, *J. Am. Chem. Soc.* **2011**, *133*, 8005.
[20] D. T. Cromer, K. Herrington, *J. Am. Chem. Soc.* **1955**, *77*, 4708.
[21] H. Tian, X. Yang, R. Chen, R. Zhang, A. Hagfeldt, L. Sun, *J. Phys. Chem. C* **2008**, *112*, 11023.
[22] A. Listorti, B. O'Regan, J. R. Durrant, *Chem. Mater.* **2011**, *23*, 3381.
[23] J. Krüger, U. Bach, M. Grätzel, *Adv. Mater.* **2000**, *12*, 447.
[24] S. Rühle, M. Greenshtein, S. G. Chen, A. Merson, H. Pizem, C. S. Sukenik, D. Cahen, A. Zaban, *J. Phys. Chem. B* **2005**, *109*, 18907.
[25] S. S. Pandey, K. Y. Lee, A. Hayat, Y. Ogomi, S. Hayase, *Jpn. Soc. App. Phys.* **2011**, *50*, 06GF08.
[26] M. Pastore, S. Fantacci, F. De Angelis, *J. Phys. Chem. C* **2010**, *114*, 22742.
[27] S. Meng, E. Kaxiras, *Nano Lett.* **2010**, *10*, 1238.
[28] G. Kresse, J. Hafner, *Phys. Rev. B* **1993**, *47*, 558.
[29] J. P. Perdew, J. A. Chevary, S. H. Vosko, K. A. Jackson, M. R. Pederson, D. J. Singh, C. Fiolhais, *Phys. Rev. B* **1992**, *46*, 6671.
[30] S. Meng, E. Kaxiras, *J. Chem. Phys* **2008**, *129*, 054110.
[31] S. Meng, J. Ren, E. Kaxiras, *Nano Lett.* **2008**, *8*, 3266.